Università degli Studi di Padova
Dipartimento di Fisica ed Astronomia
"Galileo Galilei"

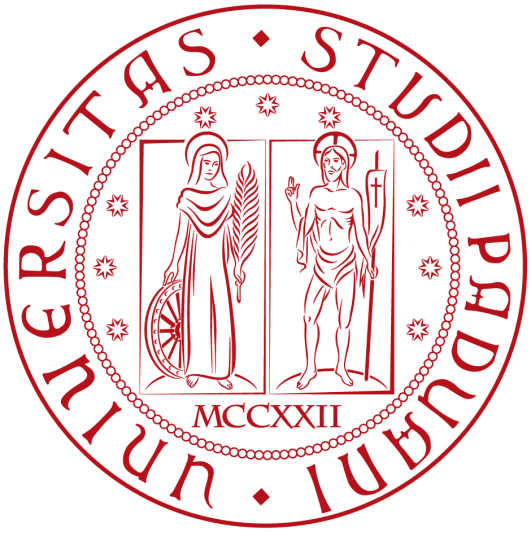

Tesi di laurea triennale in Fisica

Space and Time Clustering of High-Energy Photons detected by the Fermi LAT

Laureanda: Valeria Milotti

Relatore: prof. Denis Bastieri

Co-relatore: dott.ssa Sara Buson

Contents

Chapter 1

Active Galactic Nuclei and Diffuse Radiation

1.1 Active Galactic Nuclei

Active Galactic Nuclei (AGN), the most luminous known persistent sources of electromagnetic radiation, are among the most mysterious objects in the universe, and our knowledge of them, even after seventy years of studies, is sketchy at best. An AGN is, by definition, an astronomical object at the centre of a galaxy, whose luminosity is bigger than that of its host galaxy. These fascinating objects are still, at present, a puzzle to astronomers and physicists: it is believed that understanding them may be essential to expand our knowledge about the formation and evolution of our universe.

As in every other field of science, the first attempt at comprehension has been to divide these objects into categories, trying to figure out a unifying pattern in order to find which characteristics are common to various active galactic nuclei and whether there can be a single model that successfully predicts AGN structure and behaviour, a goal made more difficult by the vast number of phenomena observed in different wavebands. Over the years, many catalogues have been and are still being submitted, many of which use the same terminology to describe similar objects but with slightly different features.

Recent breakthroughs have been made possible by evolutions in the technology of high-energy detectors. The orbiting laboratories, first EGRET and then LAT, have allowed to discover and identify new sources, most of which were active galactic nuclei. Their work is now complemented by high-energy ground observatories, such as MAGIC, VERITAS, HESS and Cangaroo, which operate at energies above ~ 100 GeV.

Evidence suggests that nuclear activity may be a step in the evolution of the host galaxy. Exactly what triggers the nuclear activity of a galaxy, what determines the kind of evolution it will have, and what "switches it off" are questions still under study and debate.

1.1.1 Structure of an AGN

The leading hypothesis today is that AGN all present a rather complicated structure and that the abundance of phenomena observed is due to the different angle of view from which we observe them. The modern unifying theory describes AGN as composed by a very complicated structure, represented in Fig. 1.1, made of various elements, some of which could be absent in some type of AGN.

Cosmic observations tell us that many of the known galaxies, our Milky Way included, harbour a supermassive black hole at their center, which usually constitutes half a thousandth of the mass of the host galaxy [3]. This does not mean, though, that every galactic black hole is active: in fact, only about 1% of the observed galaxies have an active nucleus. In the case of AGN, this **nucleus** tends to be around $10^6 - 10^9 M_\odot$, which means that the host galaxies must have comparable masses. The black hole has never been seen directly through observation.

Around the nucleus, an **accretion disk** is present, made of material orbiting the center. Dissipative processes present in the disk cause matter to collapse inwards and heat up, and angular momentum to be transported outwards. The excess of angular momentum causes the nucleus to acquire spin, making it rotate fast.

At times, observation of the accretion disk is made troublesome or even impossible by the presence of a geometrically thick structure made of interstellar gas and dust, which will be called **torus** even though we cannot be sure of the form of its spatial distribution, that obscures the view of the central regions.

Another obstacle to the observation of the central region is constituted by the presence of a **Broad Line Region** and a **Narrow Line Region**: in the first (BLR), cold, dense, fast-moving material orbits the black hole at high speeds and relatively small distance, emitting at broadened wavelengths because of the Doppler effect; in the latter (NLR), cold material orbits the black hole too, but it is not as dense as in the BLR and it is at much greater distance and slower speeds, causing the Doppler effect to be less relevant than in the Broad Line Region and the emission to be at narrow wavelengths. In some cases, radiation from the BLR may be obscured by the torus, too.

Some accretion disks are able to produce, on one or both sides, **jets** of highly collimated (presumably by a strong magnetic field), relativistically accelerated material, hundreds of kiloparsecs to megaparsecs long, which in turn may power lobes. The jet production method and their composition is still unknown, as the difference between the many theoretical models cannot be resolved by present-day observations.

1.1.2 Electromagnetic emission

Active galactic nuclei, in contrast with stars which mostly emit over the optical band, emit powerfully from a very concentrated volume over the full accessible electromagnetic spectrum. The ultimate source powering their luminosity is the supermassive black hole's gravitational potential energy, which likely does not act through the nuclear fusion from which stars draw their energy. The strongly anisotropic emission of electromagnetic radiation is ascribed to the presence of the torus, which hinders the view of the central

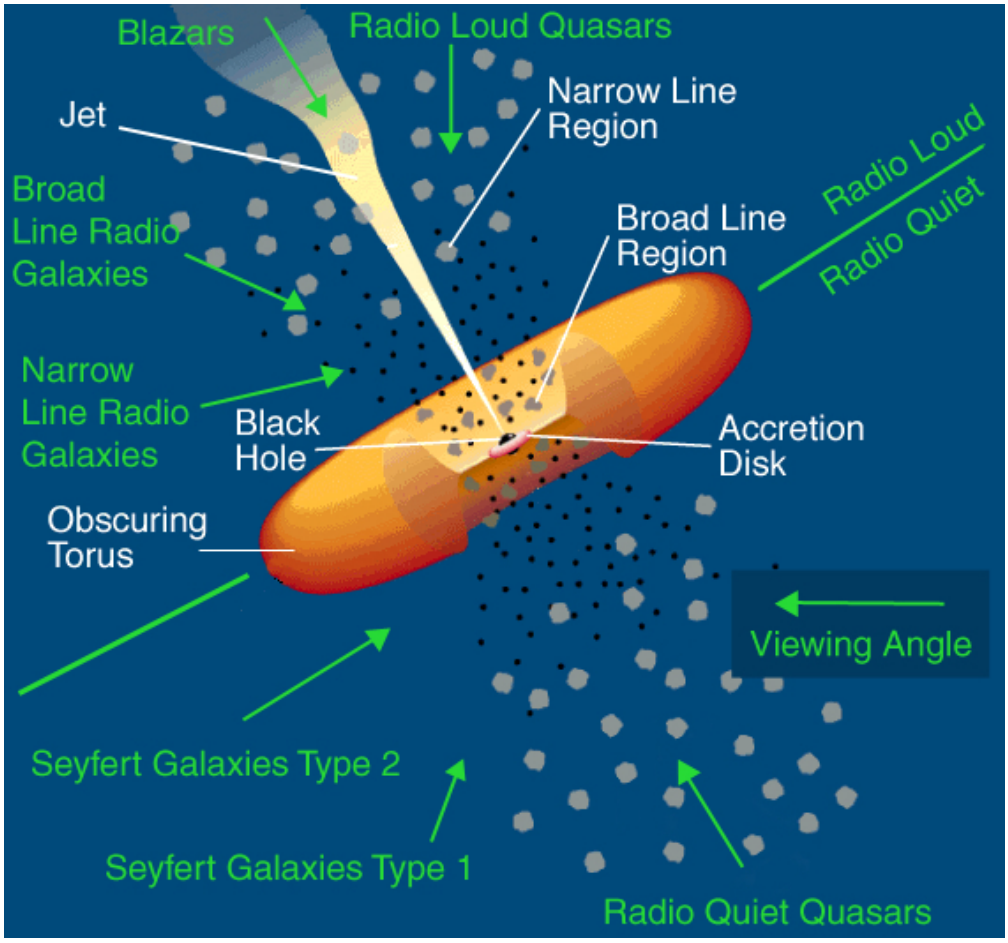

Figure 1.1: Graphic representation of an AGN with only one jet, as described by the modern Unifying Theory. The green arrows show the different classifications assigned to the AGN depending on the angle of view, according to this theory.

regions, relativistic beaming of the radiation emitted by the inner jet, and more in general to the extreme asymmetry of the model described in the previous section.

The particles constituting the accretion disk lose gravitational potential energy while collapsing towards the nucleus and in this process, as the material that composes the disk is not an ideal fluid, the friction causes the area to heat up. The hot accretion disk emits from UV to soft, and perhaps hard, X-ray radiation.

The presence of the torus causes a large fraction of this radiation to be obscured, but it is then re-radiated at longer wavelengths, most likely in the mid and far infrared. Another obstacle to the propagation of light from the accretion disk is represented by the BLR and the NLR, where the inverse-Compton scatter process takes place. The BLR and the NLR emit in the optical part of the spectrum.

By emitting synchrotron light and inverse-Compton scattered photons, jets radiate in all wavebands from radio to gamma ray, which means that AGN with jets present another source of continuum radiation for observations. When jets inflate lobes on the sides of AGN, these lobes are able to emit too, especially at radio wavelengths.

Luminous AGN present a fairly universal Spectral Energy Distribution (SED), which is the plot of data gathered studying a source that puts the logarithmic density of flux $\log \nu F_\nu$ against logarithmic frequency of the recorded photons $\log \nu$. It is used to characterise astronomical sources. For active galactic nuclei, it has two bumps, one peaking around the infrared and optical band, the other with a peak between ultraviolet and X-ray band. The less energetic peak is believed to originate from synchrotron radiation, while the higher energy one could be due to inverse-Compton scattering of the radiation, possibly the one produced by the synchrotron emission. Measuring the relative heights of the two peaks and their distance on the energy axis gives us information about the object that produced the radiation: the distance on the $\log \nu$ axis brings to the difference between the energy of the electron and the photon involved in the inverse-Compton process; the difference in height between the two peaks is the Compton Dominance (CD), that gives the density of electrons with respect to the density of photons, as it is proportional to the probability of scattering between the two populations.

1.1.3 Classification of Active Galactic Nuclei

Historically, the studies regarding active galactic nuclei consisted of two separate strands which were united at the end of the 1980s.

The first strand took into consideration the optical and X-ray spectrum, and began in 1909, when Fath and Slipher made the first recorded description of an AGN. However, the first systematic study of a class of AGN, done by Seyfert, had to wait until 1943. In the early 1960s, the discovery of quasars, objects with their high luminosities, quasi-stellar appearance and optical spectra similar to Seyfert 1 galaxies, created a wave of enthusiasm for this line of study.

The radio strand began with the first optical identifications of extragalactic radio sources in the early 1950s. The similarity between the rich emission line spectra of these "radio galaxies" and those of optical AGN was noticed already in the 1960s. Research was stimulated by the development of very long baseline interferometry (VLBI) techniques in the 1970s that allowed the inner jets of radio-loud quasars to be mapped at milliarcsecond resolution. The comparison between data taken at different times with different methods, led to the discovery of the apparent superluminal motion of some elements of the jets with respect to the host galaxy. It was realised that this is an illusion due to the jets pointing almost in the direction of the observer, realisation which led to the first unified model in 1979. This model presented many flaws, but it was of pivotal importance in setting the path for more modern and correct models.

Classification of AGN is a very complex and sometimes confusing matter. It is complicated by human and natural factors, such as the diversity in classification methods: there are many existing ways of cataloguing active galactic nuclei, which differ in subtle

or less subtle details. Moreover, attempting to force continuous sequences of properties into discrete bins often creates problems, as the characteristics of the objects under study do not present a sudden dichotomy near an arbitrary demarcation line, on the contrary most times they change gradually and continuously. Technology is also a factor in the evolution of classifications, because they change as the observation techniques become more precise and instrumentation improves, thus making us able to resolve new details which in turn can provide new insight about the object under study. Finally, the variability of the sources under study is a very important natural factor. Even though AGN are astronomical objects, and thus their lifetimes are much longer than the period they have been under study, some have been seen to undergo major changes over decades or even years. (The variability in time referred to here is permanent, not periodic.)

Despite these problems, active galactic nuclei can be classified on the basis of their radio-loudness (which is a very prominent feature of a large fraction of AGN), optical/UV morphology of their spectra, total luminosity, periodic variability, and spectral shape. There are many existing such classifications, which often share many properties with others. It is important to note that the point of classifications is not to highlight the differences between objects, but to find common behavioural patterns which may provide useful insights.

One of the historical classifications of AGN separates them in three broad classes, based on their emission in the optical-ultraviolet band:

- **Type 1 (Broad line)**: these are AGN with bright continua and broad emission lines, presumably from hot, high-velocity gas located deep in the gravitational well of the central super massive black hole.

- **Type 2 (Narrow line)**: these AGN present weak continua and only narrow emission lines. This implies that high velocity gas cannot be observed, which may be due to its absence or, as the Unifying Model theorises, to the presence of a thick wall of absorbing material blocking our view.

- **Type 0 (Unusual)**: these galaxies have very unusual spectral characteristics. Their spectra either lack strong absorption or emission features, or they present them but with very unusual traits. They are characterised by rapid variability at optical wavelengths.

- **Type 3 (Weak emission)**: this class is suggested by some authors to refer to lower luminosity AGN [2]. Type 3 will not be referred to again in this text.

A very important class of active galactic nuclei is composed by those that strongly emit radio waves, called "radio loud" nuclei, which represent about 15% of known AGN. The brightness in the radio band constitutes a rather sharp distinction between radio-loud and radio-quiet galaxies. One method employed in distinguishing between these two sets is the radio-optical ratio, which compares the relative heights of two very specific lines in the emission spectrum. For radio-quiet galaxies this ratio is usually between

0.1 and 1, while for radio-loud galaxies it falls in the range 10-1000. This method of classification leaves very few AGN in an ambiguous situation, and usually a ratio exceeding 10 is taken as the appropriate characteristic for "radio-loudness".

The properties of the radio band of the spectrum and the extended radio-emitting structures a galaxy may present also constitute possible methods for cataloguing AGN, due to the wild differences between radio-loud galaxies.

Using the two main classifications discussed above, we can create a table where it is theorised that the horizontal difference is ascribed to orientation effects and the vertical to yet-undiscovered physics [1].

Radio Emission	**Optical Emission Line Properties**		
	Type 2	*Type 1*	*Type 0*
Radio-quiet	Sy 2 NELG IR Quasars?	Sy 1 QSO	 Bal QSO?
Radio-loud	NLRG { FR 1 FR 2	BLRG SSRQ FSRQ	Blazars { BL Lac Objects (FSRQ)
	decreasing angle to the line of sight $\longrightarrow$		

It is believed that Type 2 galaxies are those which have nuclei at least partially shielded from view by the thick cloud of interstellar dust that was called torus in paragraph 1.1.1; Type 1 are tilted in such a way as to allow us to see the central region; Type 0 galaxies are believed to possess jets pointed in our general direction or almost so: the "0" comes from the small angle to the line of sight, "near 0 degrees".

Studies on the luminosity of Type 0, 1, and 2 galaxies show that indeed the energy flux coming from AGN is strongly anisotropic, thus justifying the search for a unifying model.

1.1.4 Blazars

Blazars are Type 0 radio-loud active galactic nuclei. Their characteristics are rather extreme and include:

- radio loudness;
- rapid variability, the derivative $\frac{\Delta L}{\Delta t}$ of luminosity against time is high;
- high and variable optical polarization;
- smooth, broad, non-thermal continuum: the continuous radiation is emitted by as yet unknown processes other than thermal emission;
- compact, flat-spectrum radio emission;
- superluminal motion in sources with multiple-epoch Very Large Baseline Interferometry (VLBI) maps.

The term "superluminal motion" refers to the apparent superluminal transverse speed of a radiating source moving at very high, but still subluminal, speeds at small angles to the line of sight. The source emits photons and "runs after" them, strongly reducing the time interval separating any two events in the observer's frame, giving the impression of faster-than-light motion, that is $v_{\text{apparent}} > c$. This is a direct consequence of the transformation of angles in special relativity. Moreover, an observer located near the path of the source observes a more intense emission than if the same source were at rest. This phenomenon does not apply only to blazars, but blazars tend to have the largest apparent velocities, in agreement to the hypothesis of jets almost aligned to the line of sight.

Strong relativistic beaming is thought to explain also the rapid variations in luminosity, the high polarization and high luminosity observed in blazars.

The Spectral Energy Distribution of blazars presents two separate, very broad peaks. The lower energy peak goes from radio to optical, sometimes even to X-rays, and it is thought to arise from synchrotron radiation, while the higher frequency peak, going from X-rays upwards, probably results from inverse Compton scattering, according to the more general model developed for AGN.

Blazars are further divided into two subclasses: Flat Spectrum Radio Quasars (FSRQ) and BL Lacertae (BL Lac) objects. These subclasses have similar observational properties, but differ in emission lines, namely, they are a very strong feature in the spectra of FSRQs, while BL Lac spectra lacks them entirely or present them only weakly. Moreover, BL Lac objects have, on average, higher polarization than FSRQs.

Being the type of active galactic nuclei with the greatest emission in the gamma-ray band, all new sources found and identified by EGRET were blazars. For the same reason, they represent most of the sources (57% of the observed sources according to the two-year catalog) identified by *Fermi*, and the majority of the 31% yet unidentified sources present blazar-like characteristics.

Some of the observed blazar spectra reach such high energies that the emitting source can be observed above the TeV. It is very difficult to build efficient detectors for photons this energetic, so TeV-spectrometry as a new branch of observations has only arisen in the last few years. TeV photons are observable from the ground thanks to the shower of particles they create as they interact with the higher levels of the atmosphere. TeV telescopes also have a very high angular resolution, but they can only cover a very little portion of the sky at a time. This is why GeV observatories have the important rôle of *scouts* in the monitorship of the high-energy sky: having a wider field of view, they can find potential sources in shorter lapses of time and suggest candidate sources for the TeV telescopes to observe.

1.2 The Cosmic Gamma-Ray Background Radiation

Observations made first with the Energetic Gamma Ray Experiment Telescope in the last decade of the twentieth century, then with the Large Area Telescope aboard the *Fermi* satellite in the last six years, have allowed astronomers and astrophysicists to produce all-sky maps of the gamma-ray band of the spectrum. It was therefore discovered that there is a diffuse gamma radiation flux, isotropically distributed. This **cosmic gamma-ray background radiation**, also known as **Diffuse Extragalactic Gamma-Ray Radiation**, is part of the diffuse extragalactic background radiation, the diffuse photon field of extragalactic origin that fills our Universe, with energies that span from $\sim 10^{-7}$ eV to ~ 100 GeV.

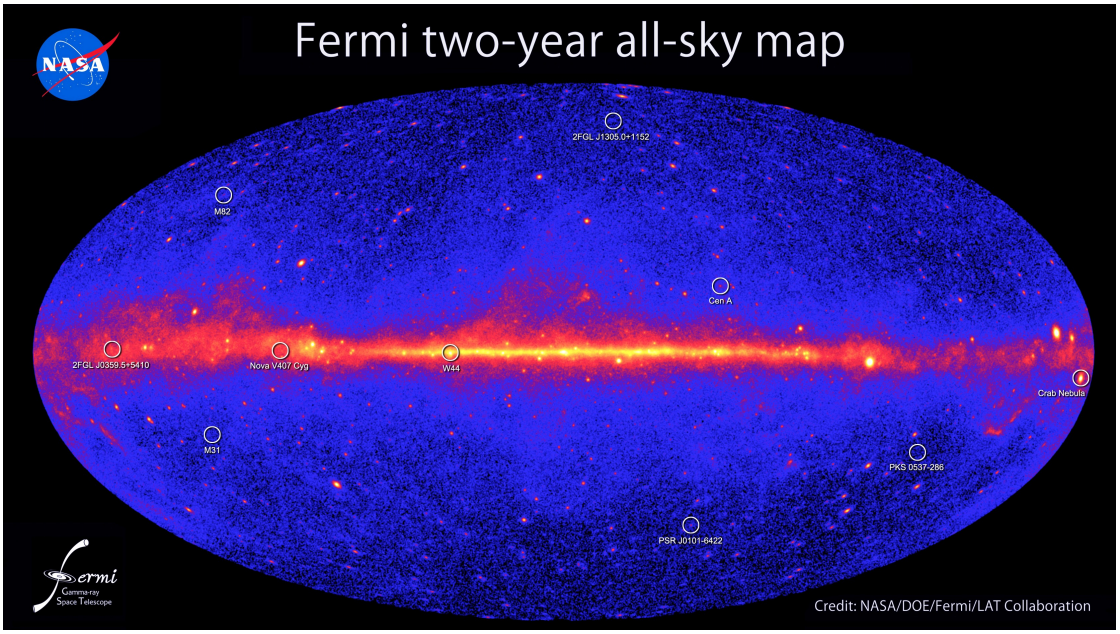

Figure 1.2: All-sky map of gamma radiation produced with data taken by *Fermi* in the first two years of mission. The colour scale represents a binned subdivision of the sky, where the warmer colours indicate where more photons originated. The diffuse cosmic gamma-ray background radiation is "visible" in the dark blue colouring.

The cosmic gamma-ray background radiation is believed to originate from three causes.

First of all, as active galactic nuclei are the only known persistent sources of continuous gamma-ray emission, there surely is a component of background radiation composed of photons originating from AGN too far to be resolved. Only less than one-quarter of the gamma-ray flux, though, can be attributed to unresolved discrete sources.

Another fraction of the flux is made of fossil radiation, which is theorised to be a truly diffuse component [7]. The shock waves induced by gravity during the formation

of aggregates of galaxies are thought to have produced a population of highly relativistic electrons, which may then have Compton-scattered with a small fraction of the Cosmic Microwave Background photons, boosting them up to gamma-ray energies.

Finally, it is believed that studying the diffuse extragalactic gamma-ray radiation may uncover new physical phenomena hidden in the bulk of the background radiation. For example, one of the objectives of the Fermi Gamma-Ray Space Telescope is to look for evidence proving or disproving the existence of Dark Matter.

So far, study of the cosmic gamma-ray background radiation has led, together with the finding of several previously-unknown galactic and extragalactic sources, to astounding discoveries, such as the detection of emitting lobes at the galactic north and galactic south of the centre of our galaxy, which may imply that our galaxy was once active.

Chapter 2

Fermi Gamma-Ray Space Telescope

The *Fermi Gamma-Ray Space Telescope*, formerly called the *Gamma-ray Large Area Space Telescope* (GLAST), is a satellite launched in 2008. It is the result of a vast collaboration of astrophysicists and particle physicists from all over the world, with contributions from scientists and institutions in Italy, the USA, France, Germany, Japan and Sweden. The satellite represents the latest stage in the evolution of orbiting instrumentation studying the most energetic part of the electromagnetic spectrum. Its performances were tested both with experiments performed in facilities on the ground and by computer simulations. Its precious cargo is composed by two instruments: the primary one is the Large Area Telescope (LAT), aided by the presence of the Gamma-ray Burst Monitor (GBM).

In the six years elapsed since its launch, *Fermi* has led to the discovery of hundreds of previously unknown sources and the identification of many of the already-known ones.

2.1 *Compton Gamma Ray Observatory* and EGRET

The precursor of the *Fermi* satellite was the *Compton Gamma Ray Observatory*, put into orbit in 1991, decommissioned in 2000, when it was de-orbited. It was the second of the four "Great Observatories" launched by NASA, the others being the *Hubble Space Telescope*, the *Chandra X-ray Observatory*, and the *Spitzer Space Telescope*. Its payload consisted of four scientific instruments, each of which led to important discoveries:

BATSE - Burst and Transient Source Experiment, (range: 25 keV - 10 MeV) studied gamma-ray bursts, for a total of about 2700 detections. Using data taken by BATSE, it was demonstrated that gamma bursters are distributed isotropically, which proved wrong both the hypothesis of bursters concentrated inside our galaxy, and the hypothesis that gamma-ray bursts were produced by neutron stars surrounding galaxies in a gigantic halo;

EGRET - Energetic Gamma Ray Experiment Telescope (range: 20 MeV - 30 GeV). It produced the first all-sky map of gamma radiation, which allowed scientist to produce new catalogues of astronomical gamma-ray emitting objects.

COMPTEL - Imaging Compton Telescope (range: 0.75 - 30 MeV), which mapped the distribution of the radioactive isotope ^{26}Al;

OSSE - Oriented Scintillation Spectrometer Experiment (range: 50 keV - 10MeV), which, by detecting the gamma rays produced in the annihilation of positrons with electrons, found evidence of high energy particles entering the Sun and exciting nuclei.

Of these instruments, EGRET is the direct predecessor to *Fermi*'s Large Area Telescope, and it provided the highest energy gamma-ray window for the *Compton Observatory*. Even though its sensitivity was fifty times worse than LAT, it was 10 to 20 times larger and more sensitive than previous detectors operating at such high energies: it made possible detailed observations of high-energy processes associated with diffuse gamma-ray emission, gamma-ray bursts, cosmic rays, pulsars, gamma-ray blazars, high-energy solar flares, and diffuse radiation from our Galaxy and beyond that had a momentous impact on theories about the high-energy universe. Within the first four years of mission, EGRET allowed the production of all-sky maps of incoming gamma-radiation and of a catalogue of 271 newly observed astronomical objects, 66 of which were blazars.

2.2 The *Fermi* instrumentation

The instrumentation aboard *Fermi* comprises two instruments, each of which operates at high energy range.

2.2.1 Large Area Telescope (LAT)

The **Large Area Telescope (LAT)** is the main instrument aboard *Fermi*. Its operating range is 20 MeV - 300 GeV, much wider than EGRET's (20 MeV - 30 GeV). It presents many more improvements with respect to EGRET, such as a larger field of view, improved angular and energy resolutions, and lower dead-time. Moreover, in contrast with EGRET, it has the advantage of not being dependent on consumables such as gas. It is designed to measure energy, direction, time of arrival of incident gamma-rays, while rejecting the background signals originated from charged cosmic rays.

The orbiting mode of *Fermi* has been designed to take full advantage of the wide field of view the LAT has, the so-called "scanning" mode, in which the normal to the front of the instrument (z-axis) on alternate orbits is pointed to $+35°$ from the zenith direction and towards the pole of the orbit and to $-35°$ from the zenith on the subsequent orbit. This allows to have an almost uniform exposure of the sky every two complete orbits. The observatory can also be inertially pointed towards a fixed point in the event of interesting phenomena.

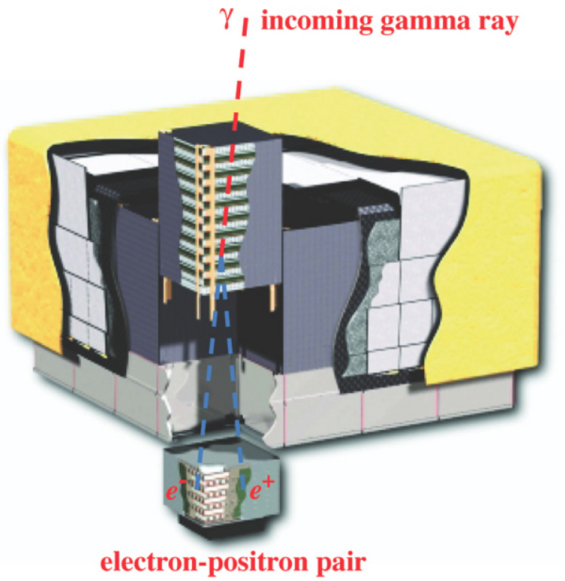

Figure 2.1: Schematic diagram of the LAT. The yellow cover represents the anticoincidence detector. The structure of a single module is visible: the tracker is the upper part, where the incoming gamma-ray interferes with a high atomic number material, while the calorimeter, whose task is to measure the energy of the electrons and positrons resulting from the interaction of gamma-rays with the tracker, is the lower part.

High-energy gamma-rays cannot be reflected or refracted; they interact with matter by the conversion of the photon into an $e^+ - e^-$ pair. The LAT is therefore a pair-conversion telescope with a precision converter-tracker and calorimeter, each consisting of a 4×4 array of 16 modules supported by a low-mass aluminum grid structure.

The LAT's tracker array is covered by a segmented anticoincidence detector (ACD) in order to distinguish between high-energy photons which then create an $e^+ - e^-$ pair inside the instrument, and already ionized particles, such as charged cosmic rays, which constitute noise. A programmable trigger and data acquisition system utilizes prompt signals available from the tracker, calorimeter, and ACD subsystems to form a trigger.

The Tracker

The tracker is the part of LAT where the conversion of the photon into a pair of charged particles, namely an $e^+ - e^-$ pair, takes place. The tracker, thus, has the double function of inducing the photon's decay and tracing the path of the resulting electron and positron. Moreover, the pair conversion signature is also used to help reject the much larger background of charged cosmic rays.

Each module of the tracker is a stack of 19 trays, which act as support for converter foils and detectors, and allow the signal from the detectors to be transmitted to the

computer by the front-end electronics. All trays are of similar construction, but the top and bottom trays have detectors only on the inward face.

The converter foils are thin Tungsten sheets, they are 16 and inserted only in the upper trays. Tungsten ($Z = 74$) was chosen because of its high atomic number, as probability of interaction between a photon and a material grows strongly with Z. The Tungsten converter foils in the first 16 planes lie immediately above the upper detector layer in each plane, while the lowest two detecting planes have no tungsten foil.

The trays have two detector planes, one on the upper face, one on the lower face. The detector planes are composed by adjacent single-sided Silicon Strip Detectors (SSD), with all the strips on a single tray laid in the same direction. In order to have a two-dimensional detecting plane, alternate trays are rotated of 90° with respect to each other, so that the lower strips of the upper tray form an (x, y) measurement plane with the orthogonal detector layer on the top of the tray just below.

A tension gradient is constantly applied to each SSD, and the transit of a charged particle such as an electron or a positron creates fluctuations in this gradient. This method is very convenient as it is extremely precise (bad channel rate less than 0.01%) and eliminates the need of a trigger, reducing the instrument's dead time.

The probability distribution for the reconstructed direction of incident gamma-rays from a point source is referred to as the *point-spread function* (PSF). In order to obtain an optimal PSF, the directions of the e^+ and e^- should be measured immediately after the photon conversion, so as to avoid scattering on multiple foils. Thus, the SSD layers have to be situated as close as possible to the nearest converter.

The designing of LAT had to balance two needs: to achieve a good PSF at low energy, where the PSF is determined primarily by the $\sim \frac{1}{E}$ dependence of multiple scattering, by using thin converters, *versus* the need for converter material to maximize the effective area, important at high energy.

The tracker provides the principal trigger for the LAT, where noise is minimized by using as first-level trigger the coincidence of a signal in successive layers (typically three (x, y)-planes). The 16 modules operate independently, providing much redundancy, as does the multilayer design of each module.

The Calorimeter

The calorimeter has two main purposes:

1. to measure the energy released by the electromagnetic particle shower that results from the pair conversion;

2. to image the shower development profile, which contributes significantly to background rejection (especially at high energies) and acts as estimator of the shower energy leakage fluctuations.

Each calorimeter module has 96 CsI(Tl) crystals, optically isolated from each other, arranged horizontally in eight layers, with crystals in each layer perpendicular to the crystals of the adjacent layers. The total vertical depth of the calorimeter is 8.6 radiation

lengths (for a total instrument depth of 10.1 radiation lengths), where a radiation length is the spatial length an electron travels inside a material before its energy is reduced by a factor $\frac{1}{e}$. Although the calorimeter is only 8.6 radiation lengths deep, the longitudinal segmentation enables energy measurements up to a TeV.

The three-dimensional spatial reconstruction of the shower uses the physical location of the crystal in the array to obtain two of the three spatial coordinates needed, while the third is inferred by measuring the scintillation light asymmetry at the ends of the crystal along the longer axis. This method provides sufficient information to allow spatial imaging of the shower and accurate reconstruction of its direction, which have pivotal importance in background rejection.

The resolution in measuring the scintillation light asymmetry at each end of the crystal is proportional to the deposited energies, becoming increasingly precise at higher energies.

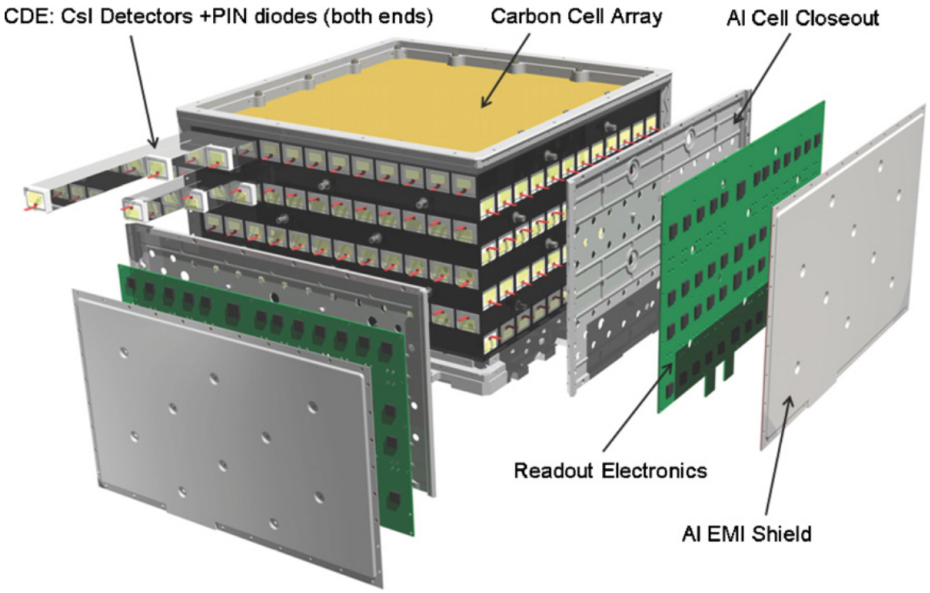

Figure 2.2: LAT calorimeter module. The 96 CsI(Tl) scintillator crystal detector elements are arranged in eight layers, with the orientation of the crystals in adjacent layers rotated by 90°.

The Anti-Coincidence Detector (ACD)

The purpose of the Anti-Coincidence Detector (ACD) is to detect the arrival of charged cosmic rays, which constitute the bulk of the noise for the Fermi LAT. The ACD is made of plastic scintillator tiles, which were chosen for their good performances, already tested in space, and their low cost; the light emitted is gathered and passed to photomultiplier

tubes in order to boost the signal. The efficiency of the ACD may be compromised by the "backsplash effect", that is the creation of secondary particles in the decay shower when the energy of the incoming photon exceeds 10-20 GeV. These particles are mostly photons, which can interact via Compton scattering with the ACD, thus creating false background which may bring to the rejection of viable data. In order to bring this problem to a minimum, the ACD is segmented so that only the portion close to the candidate photon may be considered, reducing the backsplashing area.

Data Acquisition System (DAQ) and Trigger

The Data Acquisition System (DAQ) provides onboard processing of data gathered by the other subsystems, applying the multilevel event trigger and filter algorithms in order to reduce the number of events transmitted to the ground, and is an onboard science analysis platform for the rapid search of transients. Filtering the massive bulk of data gathered by onboard instrumentation is pivotal because the bandwidth used for transmitting signals to the ground is limited and it wouldn't be able to transfer the enormous amount of information.

2.2.2 Gamma-ray Burst Monitor (GBM)

The **Gamma-ray Burst Monitor (GBM)** has an operating range between 8 keV and 40 MeV. It complements the observations of the LAT for high energy transients, being sensitive to low-energy gamma-rays and X-rays. It is the successor of the BATSE, having, though, the possibility to study a wider energy range.

The structure of the GBM is made of two sets of detectors:

- 12 sodium iodide (NaI) scintillators, sensitive to an energy range spanning from a few keV to about 1 MeV. Its purpose is to provide burst triggers and location.
- two cylindrical bismuth germanate (BGO) scintillators, whose detecting range goes from ∼150 keV to ∼30 MeV, providing the range bridge between the NaI scintillators and the LAT.

The GBM gathers data continuously, in order to provide information about the development of a Gamma Ray Burst even before the trigger activation. After the trigger, the processors of the GBM rapidly calculates the position and spectral information about the transient. The data is immediately processed by *Fermi*'s hardware, which can, if necessary, move the satellite in order to keep the origin of the burst inside LAT's field of view.

2.2.3 *Fermi* Data Processing

The majority of signals detected by the instrumentation is background noise, caused by charged particles and by gamma rays due to the Earth's albedo. As the bandwidth with which the signals are transmitted to the ground is limited, the action of the instruments' triggers is very important in reducing the bulk of data recorded and in minimizing the

effects of background particles on the deadtime associated with the LAT. Moreover, the raw data gathered by the LAT and the GBM undergoes the first science processing onboard. This first analysis consists of algorithms to:

1. select gamma-ray candidate events, so as to remove the background noise as much as possible, but without rejecting celestial gamma-ray events;

2. reconstruct directions of gamma-ray candidate events;

3. search for and localise high energy transients. In the event a transient is localized, the output of this processing can trigger an autonomous repointing of *Fermi* so as to keep the area inside the LAT's FoV.

The output is then downlinked to ground facilities every two orbits, that is every three hours, where it undergoes further automated processing. The purpose of this last automated analysis is to distinguish between background events and gamma-ray events and minimize the impact of backgrounds on gamma-ray science.

The product of this series of analyses is divided into classes with different background rejection, each serving different purposes of study, differentiated by an increasingly tighter requirement that the candidate photon events in both the tracker and the calorimeter behave as expected for gamma-ray induced electromagnetic showers. The differences among analysis classes are largest at low energies, where the interference of charged particles with the calorimeter is highest.

2.3 The objectives of the *Fermi* mission

During the first year of operation alone, *Fermi* detected more than a hundred times more gamma-rays than EGRET did in nine years of activity. The superiority with respect to previous instruments and the wider field of view to high-energy ground-based observatories allow *Fermi* to address a number of important scientific objectives, including the following:

Determine the nature of unidentified high-energy gamma-ray sources

Of the sources observed by EGRET, only 66 were identified at high confidence and 27 were classified as low-confidence blazars. The other 170 new sources present in the catalog were left unidentified. Because of its much narrower PSF and larger field of view, and thus to smaller error boxes than were possible with EGRET, *Fermi* has allowed to make significant progress in source localization and identification.

Understand the mechanisms of particle acceleration operating in celestial sources and the origin of cosmic rays

The structure of active galactic nuclei appears to be extremely complicated, and there are still many open questions about it. The ones *Fermi* tries to answer are those about

the gamma-ray emission and about the gamma-ray emitting parts of the AGN. Most of the gamma-rays are emitted by non-thermal processes from narrowly beamed relativistic jets, boosted in the forward direction. The means by which the jets are collimated, their composition, the production of high-energy photons are still rather mysterious.

Finally, pulsars represent point sources of gamma-rays belonging to our Galaxy, and *Fermi* has been studying their pulse profiles and phase-varying spectra.

Study the high-energy behaviour of Gamma-Ray Bursts and transients

Gamma-Ray Bursts are thought to be the most energetic explosions in the galaxy, releasing in an instant unthinkable amounts of energy. Previously to the launch of *Fermi*, knowledge about high-energy Gamma-Ray Bursts (GRBs) mainly came from observations made with the instruments aboard the *Compton*, especially EGRET and BATSE.

There are two types of GRBs: long duration GRBs ($\tau > 2s$), which are thought to be the result of massive star collapse and black hole formation, and short duration GRBs, that arise from the coalescence of compact objects. Both kinds of bursts were observed by EGRET and BATSE, but observations were hindered by EGRET's deadtime ($\sim 100ms$), which was comparable to or even longer than the duration of the pulse, making it impossible to study the prompt time evolution of the burst. The wider field of view and the dramatically lower deadtime of the *Fermi* instrumentation has made possible the study of the prompt component in the evolution of the bursts. According to theoretical expectations, the LAT detects about a burst per month, while the lower-energy GBM detects about 250 burst per year.

Search for signatures of dark matter annihilation or decay and understand the diffuse gamma-ray emission from the Galaxy

EGRET observations were hindered by its relatively small effective area above ~ 10 GeV and the interference of the backsplash effect at high-energies which caused the rejection of some gamma-ray triggers. The design of *Fermi* eliminates the backsplashing problem and its capabilities for searching for dark matter were widely discussed before launch.

Determine the attenuation of high-energy gamma-rays as a function of cosmological redshift

The extragalactic background light (EBL), in the band comprising near-UV, optical, and near-infrared, is accumulated radiation from the era of star and galaxy formation. Observations of the EBL suffer huge systematic uncertainties due to the presence of luminous sources on the celestial sphere. Because of this, studying the attenuation in the gamma-ray flux caused by the absorption of high-energy gamma-rays via pair production in the EBL, gives the opportunity to probe the EBL at redshifts greater than 0.5.

Chapter 3

Data Analysis

The analysis in this thesis concentrates on data taken by *Fermi*-LAT at high-energy coming from the cosmic background radiation. As it has been argued, analysing the background radiation can lead to many interesting results. The objective of this work is to cluster photons detected by the LAT using constraints on space and time, in order to detect new potential sources hidden in the cosmic gamma-ray noise. The cluster analysis was executed using also a temporal constraint in order to bring to light possible variations in the local flux of photons, which may be due to flares from active galactic nuclei.

3.1 Event selection

The events taken into consideration were those gathered by *Fermi*'s LAT with energies above 50 GeVs and with galactic latitude, b, above $20°$ and below $-20°$, over a period of about six years. The LAT's PSF allows, at such high energies, to have an excellent angular resolution, of about 0.1 degrees.

Since there are fewer incoming photons at higher energies, the number of events to be analysed was relatively small: applying only the energy selection, the number of events to be analyzed was about 51000. The second cut (over b) was applied in order to exclude from the analysis the data gathered from the Milky Way, which dilutes the diffuse component, harbours point-sources of gamma-rays such as pulsars, and present in itself a diffuse source. This second restraint dramatically reduced the number of events under analysis, bringing the number to about 18400.

The most logical assumption to make is that the mean number of collected photons arrived in a fixed, small interval of time is constant and very small, moreover the arrival of each photon is independent of the photons observed before it. These two hypotheses lead us to theorise that the arrival of photons follows a Poisson distribution, and the time elapsed between two consecutive events follows an exponential distribution.

This, though, is not completely true for the data in question, because part of the observed photons are emitted from point sources and are not part of the diffuse component.

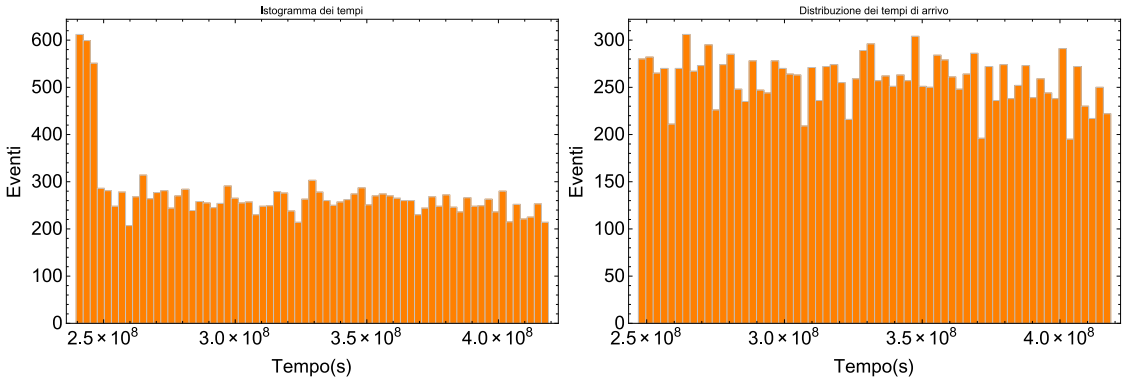

(a) All data used. The peak at a time-of-mission lower than $2.47 \cdot 10^8$ is evident.

(b) Data before $2.47 \cdot 10^8$ second cut out.

Figure 3.1: Histograms of events's time arrivals, divided into intervals of thirty-one days.

The first histogram plotted the *time of arrival* of each event against the *number of events measured in an interval of time* (Fig. 3.1a) evidenced an anomaly in the data, probably due to a problem in the acquisition, as it seems that too much noise was accepted as viable data.

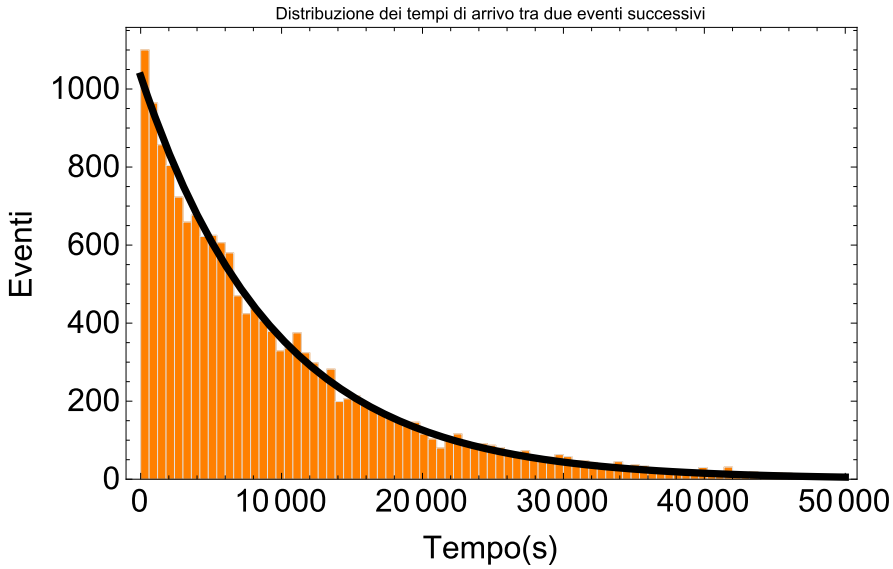

Figure 3.2: Histograms of the differences between times of arrival of successive events with the fitted exponential.

In order to clean the analysis, we introduced an additional cut by selecting only data recorded after MET $2.47 \cdot 10^8 sec$ (MET or *Mission Elapsed Time* is the number of seconds after January 1^{st}, 2001). The number of events taken into consideration lowered

to 16712, and the anomaly in time of arrival disappeared, verifying the hypothesis of a fixed mean of events measured. In this case, the time elapsed between two events followed an exponential distribution, at least qualitatively:

$$(1033 \pm 11) \cdot \exp^{-1.05 \cdot 10^{-4} \pm 0.01 \cdot 10^{-4}} \tag{3.1}$$

It must be noted that data should follow an exponential distribution if the only source present was the diffuse component (Fig. 3.2). This, though, is not our case, as there are several additional point-like sources.

3.2 Spatial clustering

The spatial clustering of events was executed by using a clustering algorithm called DBSCAN, whose first implementation was written in 1996 by Esther et al.. This algorithm needs to be fed by a list of events to analyze and two parameters, a radius ϵ and a minimum number of photons k, in order to function. The first step the algorithm takes is to compute a circle C^0 of radius ϵ around each photon in the list: if the photons inside the circle, that is the ones which are at a distance smaller than ϵ from the central photon, are $(k+1)$ or more, the photon at the center is taken as "seed" of the cluster C. The other k photons inside C^0 are then scanned as well, by tracing a circle C^m of radius ϵ around each of them. If the area $C^m \setminus C^0$ contains another k photons, the the circle C^m is added to the cluster.

As at the energies considered the LAT's Point Spread Function is of the same order of magnitude as $0.1°$, measurements of direction of arrival are very precise (at lower energies the PSF increases to the order of magnitude of 5). The radius ϵ of the seed cluster was considered to be $0.5°$, giving to each seed cluster the diameter of $1°$. Actually, as the DBSCAN algorithm is implemented to function with a flat metric, the celestial sphere was divided into ten zones, in order to keep the metric inside each zone approximately flat, and the error on distances lower than a factor 2. This means that in the most distorted parts of the zones the actual distance between coordinates were at worst double than they are in reality.

The zones into which the sky was divided were selected using galactic longitude (L) and galactic latitude (B). Together they cover all the celestial sphere minus the strip $B \in [-20°, 20°]$. There is redundancy in the subdivision in order to avoid the possibility of missing clusters near the border of each zone, and also because L and B have singularity points where the coordinates are not defined.

Zone	L (Galactic longitude)	B (Galactic latitude)
A	$[0°, 180°]$	$[+20°, +60°]$
B	$[180°, 360°]$	$[+20°, +60°]$
C	$[0°, 360°]$	$[+55°, +90°]$
D	$[0°, 90°] \bigcup [270°, 360°]$	$[+20°, +60°]$
E	$[90°, 270°]$	$[+20°, +60°]$
F	$[0°, 90°] \bigcup [270°, 360°]$	$[-20°, -60°]$
G	$[90°, 270°]$	$[-20°, -60°]$
H	$[0°, 180°]$	$[-20°, -60°]$
I	$[180°, 360°]$	$[-20°, -60°]$
L	$[0°, 360°]$	$[-55°, -90°]$

The zones C and L contained the poles, and a rotation of coordinates was required. The rotation chosen was a three dimensional rotation of a 90° angle about the x-axis, described by the matrix:

$$\begin{pmatrix} 1 & 0 & 0 \\ 0 & \cos\theta & -\sin\theta \\ 0 & \sin\theta & \cos\theta \end{pmatrix} = \begin{pmatrix} 1 & 0 & 0 \\ 0 & 0 & -1 \\ 0 & 1 & 0 \end{pmatrix} \tag{3.2}$$

After the algorithm had been applied to the transformed data, the output was transformed back to "ordinary" coordinates, using the inverse transformation:

$$\begin{pmatrix} 1 & 0 & 0 \\ 0 & \cos\theta & \sin\theta \\ 0 & -\sin\theta & \cos\theta \end{pmatrix} = \begin{pmatrix} 1 & 0 & 0 \\ 0 & 0 & 1 \\ 0 & -1 & 0 \end{pmatrix} \tag{3.3}$$

Knowing the value to be given to ϵ, the value of k had to be computed. The number of circles of radius $\epsilon = 0.5°$ one can trace on the celestial sphere is

$$N_{circles} = 4\pi \cdot \frac{1}{(\epsilon^2 \cdot \pi)} = 4\pi \cdot \frac{(180°)^2}{(0.5°)^2 \cdot \pi^3} = 52524.9 \tag{3.4}$$

Assuming all the photons considered (whose number is $N_{photons} = 16712$) to be from the background, the mean rate of arrival from each circle of radius $\epsilon = 0.5°$ is

$$\lambda = \frac{N_{circles}}{N_{photons}} = 3.14295 \tag{3.5}$$

The expected background distribution is the Poisson distribution with a mean equal to λ:

$$\left(\frac{1}{\lambda}\right)^k \cdot \frac{e^{-\lambda}}{k!} \tag{3.6}$$

The probabilities to find k random photons from the background inside the same circle of radius $\epsilon = 0.5^\circ$ have been computed:

$$k = 3 \quad \rightarrow \quad \left(\frac{1}{\lambda}\right)^3 \cdot \frac{e^{-\lambda}}{3!} = 3.90533 \cdot 10^{-3} \tag{3.7}$$

$$k = 4 \quad \rightarrow \quad \left(\frac{1}{\lambda}\right)^4 \cdot \frac{e^{-\lambda}}{4!} = 3.10642 \cdot 10^{-4} \tag{3.8}$$

$$k = 5 \quad \rightarrow \quad \left(\frac{1}{\lambda}\right)^5 \cdot \frac{e^{-\lambda}}{5!} = 1.97676 \cdot 10^{-5} \tag{3.9}$$

The probability to find a random association of $k = 3$ photons is still not excessively small ($\sim 0.4\%$), but it rapidly decreases as the parameter k increases to the values of 4 and 5 ($\sim 0.03\%$ and $\sim 0.002\%$). Thus, it seemed like good choice to take $k = 4$ and $k = 5$.

3.2.1 Time selection

After the clustering algorithm was run, both with $k = 4$ and $k = 5$, a further selection was applied by comparing the time-of-arrival of each photon belonging to each cluster with the time-of-arrival of every other photon belonging to the same cluster. This selection was applied by using a $\Delta t = 604800s$, that means that the output was generated by photons arrived within a week of each other.

The complete output was compared to a list of high-energy gamma-ray emitting sources and to a catalogue of all of *Fermi*'s already-identified sources (the preliminary 3FGL catalogue). The clusters that survived the time selection seemed all to correspond to already-known high energy sources, but to say this with certainty an analysis using the *Fermi Tools* Likelihood should be undergone. It certainly is interesting that so many sources survived, as the time selection presented a rather strong requirement. Moreover, if the likelihood analysis should confirm that the clusters found indeed correspond to a source, the arrival of more than one photon in the temporal interval Δt could be a strong indicator that the source in question has flared, or maybe even that a source which usually does not emit hard gamma-rays has, for some reason, emitted photons of energies higher than 50 GeV.

The output generated with $k = 4$ and $k = 5$, respectively, can be found in Fig. 3.3 and Fig. 3.4. It is to be noted that the clusters found in the first instance were in greater number than the ones found in the second: after the spatial selection only, the set generated with $k = 4$ contained about twice the number of clusters as the other set. The ratio of the number of elements between the two sets was greatly reduced, but not cancelled, by the time selection.

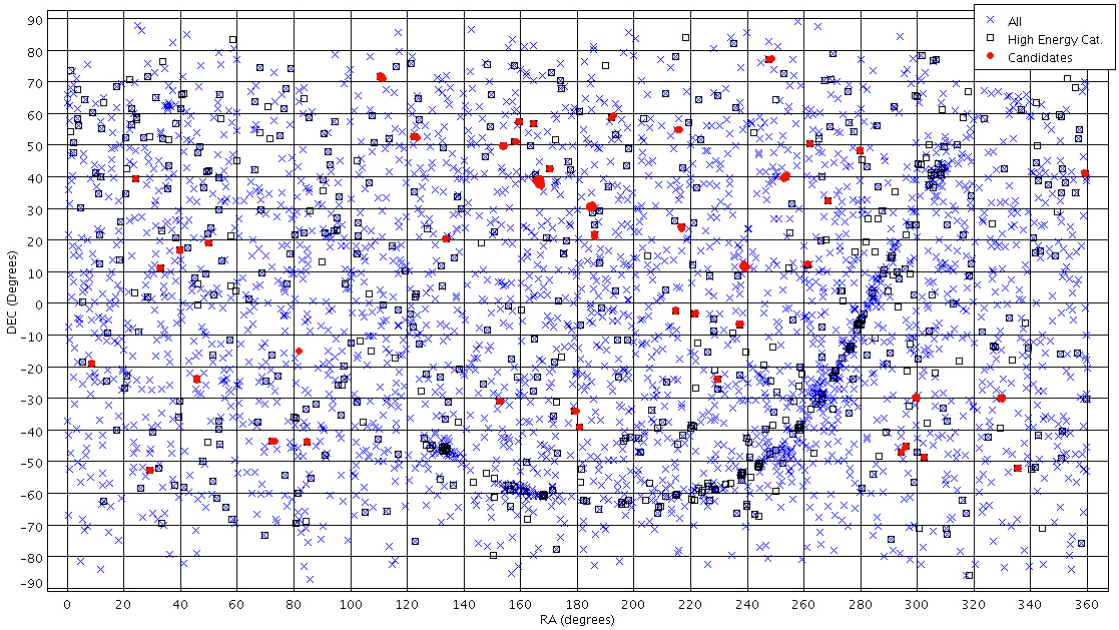

Figure 3.3: All-Sky image of the clusters found using the $\epsilon = 0.5°$ and $k = 4$ (red dots) against the sources in the high-energy catalogue (black squares) and the preliminary 3FGL catalogue (blue crosses).

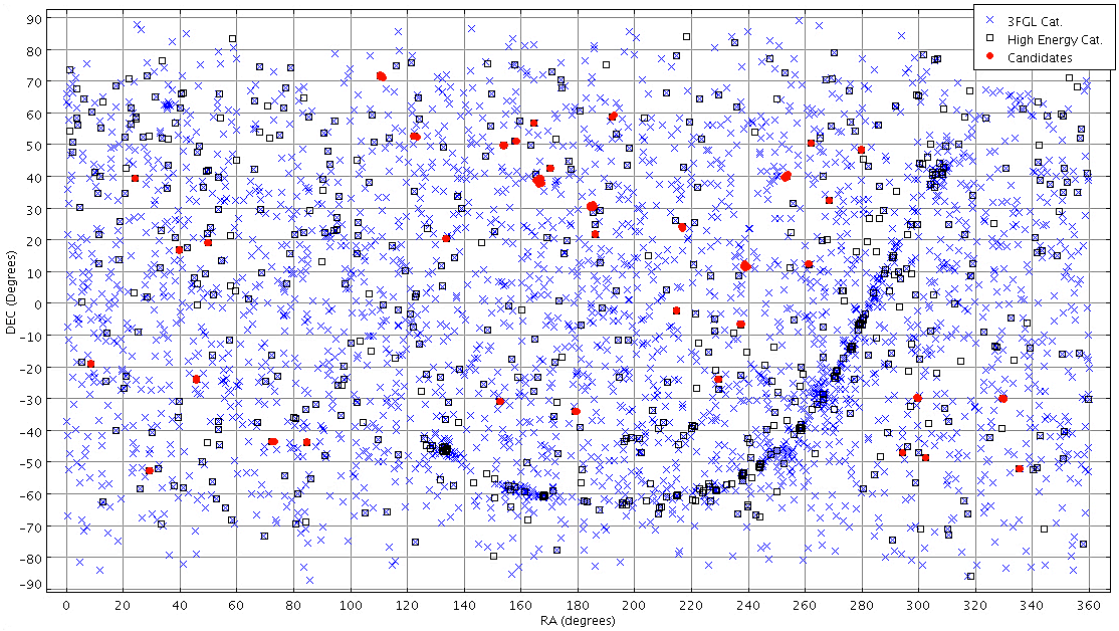

Figure 3.4: All-Sky image of the clusters found using the $\epsilon = 0.5°$ and $k = 5$ (red dots) against the sources in the high-energy catalogue (black squares) and the preliminary 3FGL catalogue (blue crosses).

3.3 *Fermi Tools* Likelihood Analysis

As the time selection did not lead to particularly interesting results, it was put aside and no time restriction on the clustered photons was considered. This time, there were several cluster which only had a correspondence in one of the two catalogues, or did not have any correspondence in either of them. One of the clusters found by the spatial analysis conducted in section 3.2 was chosen to be analysed.

The two catalogues considered do not match exactly: the preliminary 3FGL catalogue contains all sources identified until now, while the other catalogue is a list of candidate sources which emit in the higher-energy band of the spectrum, some of which still have not been officially identified. In fact, the first cluster analysed had a correspondence in the latter catalogue, but not in the first.

3.3.1 PGW_00453

The source selected to undergo the analysis was one present only in the high-energy catalogue, listed as *PGW_00453*, with no correspondence at all in the preliminary 3FGL catalogue, which means it has not, as yet, been confidently identified. In order to execute

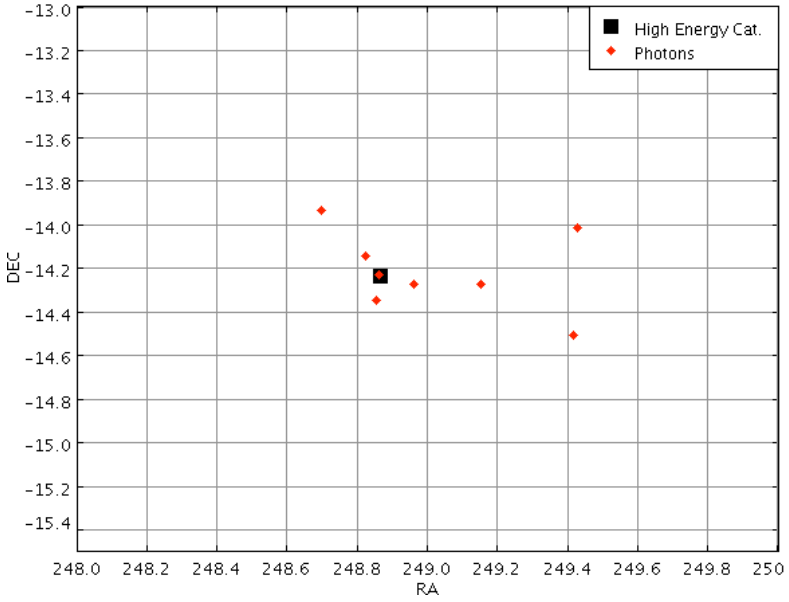

Figure 3.5: Elements of the cluster (red diamonds) around the coordinates of the source classified as PGW_00453, marked with the black square.

the *Fermi Tools* likelihood analysis, the position of the source was taken to be the one listed in the high-energy catalogue:

$$\begin{aligned} \text{Right Ascension} &= 248.8650^\circ \\ \text{Declination} &= -14.2377^\circ \end{aligned} \tag{3.10}$$

The cluster found by the clustering algorithm was relatively very big, as it comprised 8 photons, part of the data subset which had survived the selection with $\epsilon = 0.5°$ and $k = 5$, almost twice the minimum number of events needed to "seed" a cluster. The photons were clustered around these coordinates, as can be seen in Fig. 3.5. The list of photons and their characteristics can be found in Table 3.1.

Right Ascension (degrees)	Declination (degrees)	Time of arrival (seconds)	Photon Energy (MeV)
248.8624°	-14.234713°	$3.02724790805 \cdot 10^8$	66756.81
248.85384°	-14.351704°	$2.87358279401 \cdot 10^8$	302022.12
248.6992°	-13.938411°	$3.25648938073 \cdot 10^8$	63291.84
249.42844°	-14.016861°	$3.34972037078 \cdot 10^8$	208171.0
248.96086°	-14.277348°	$3.56952380103 \cdot 10^8$	88091.45
248.82419°	-14.145851°	$3.6894084514 \cdot 10^8$	237758.48
249.41759°	-14.5111°	$3.91508370688 \cdot 10^8$	63633.363
249.15125°	-14.276224°	$3.99222448688 \cdot 10^8$	84382.164

Table 3.1: Characteristics of the photons composing the cluster which had a correspondence in PGW_00453

The data used for the analysis still belonged to the high-energy list of photons selected in section 3.1. The Region Of Interest (ROI), that is the area considered for the analysis, extended over a circle with radius 15° and centered on (3.10).

First of all, a counts map for the ROI was created: the area was divided into bins and a value was assigned to each bin, proportional to the number of events belonging to the area covered by the bin. The result can be seen in Fig. 3.6. Near the boundary of the ROI another source was present, which had been already identified in the preliminary 3FGL catalogue as 3FGLJ1714.1-2029, with a TS of about 27.

The likelihood analysis made by the *Fermi Tools* finds the ratio between the logarithmic probability of the positive existence of the source against the logarithmic probability of its non-existence. The value given by the program gave the source's existence at TS = 18.06, with a flux equal to $1.77 \cdot 10^{-9} \pm 6.70 \cdot 10^{-9}$.

The data were further submitted to the *Fermi Tools*, and the "best" coordinates for the center of the potential source were determined to be:

$$\begin{aligned} \text{Right Ascension} &= 248.866° \\ \text{Declination} &= -14.2368° \end{aligned} \tag{3.11}$$

The likelihood analysis was repeated using the new coordinates (3.11), and this time the result was TS = 18.022. A TS so high means that the existence of a source at the coordinates given is much more probable than its non-existence.

Then, the fitted model of the ROI found by the likelihood analysis was compared to the actual map of photons given by observations, by subtracting the latter from the first.

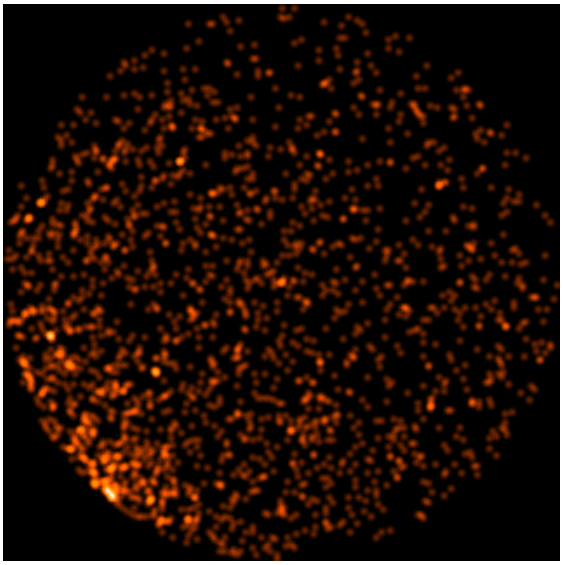

Figure 3.6: Counts map of the ROI.

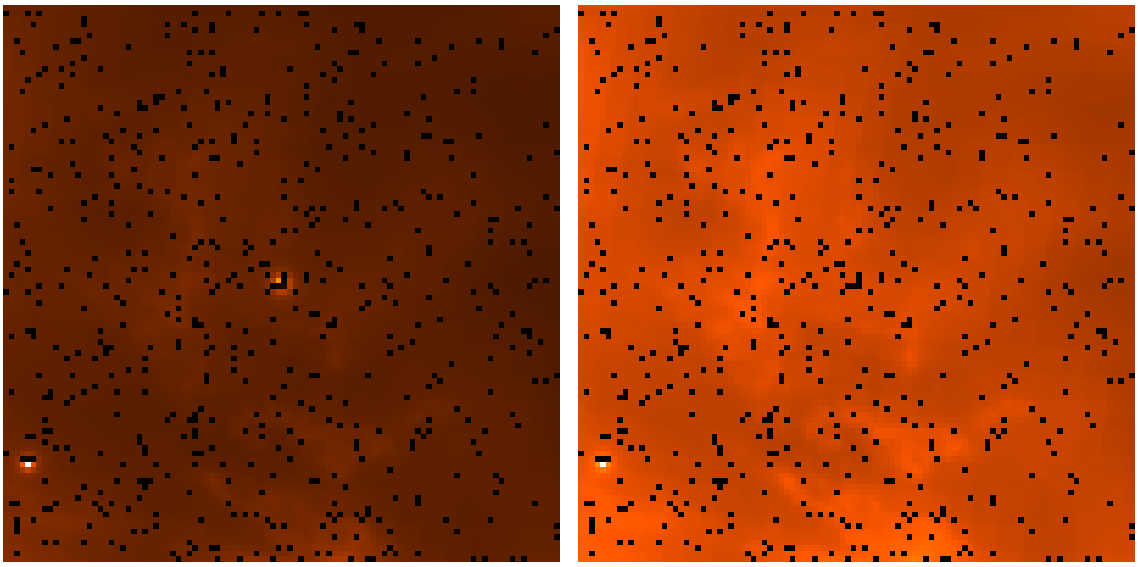

(a) Fitted with the source. (b) Fitted without the source.

Figure 3.7: Maps of the residuals. On the left the fit was executed considering the source, on the right the source was taken out of the parameters.

The result was a map of residuals of the ROI, that is the difference between the number of photons predicted by the model and the actual observations for each bin the ROI was divided into. The map of the residuals gave a result which was in partial disagreement to the likelihood analysis, as the photons expected from the fitted model were many more than the observed ones (white dot at the center of Fig. 3.7a).

A new model was fitted, one where the source at coordinates (3.11) was considered as non-existent, and this time the fluctuations in the map of the residuals were closer to the expected value of 0 (see Fig. 3.7b). The method of analysis involving the maps of the residuals thus favours the non-existence of the source.

3.4 Final Observations

The empirical process of analysis introduced in section 3.2 has proven to be valid in finding already identified sources. Interesting future developments might include a further expansion of the method, by feeding the DBSCAN algorithm with pre-processed non-flat metrics, in order to eliminate the multiplying factor introduced by considering the patchwork of semi-flat zones instead of the more correct, spherical area encompassing all zones at once.

Another implementation possible would be to refine the time selection, maybe by carrying out the temporal clustering before the spatial one.

Moreover, all results from the previous processes, whose results are ultimately qualitative, should be subject to the more accurate *Fermi Tools* analysis, which instead gives quantitative output.

The analysis undertaken in section 3.3.1 was executed only on data with energies higher than 50 GeV and the *Fermi Tools* analysis gave conflicting results: the likelihood analysis gave the existence of the source as probable (TS=18.02), while the map of residues stated the contrary. This dichotomy may be resolved by repeating the analysis with lower energy requirements, by using data with energies higher than 20 GeV, or even 10 GeV. Completely eliminating the energy requirements may be counter-producing, as, if the source did indeed exist, it would be very weak and by considering the whole energy band its emission may be drowned into the background noise.

Bibliography

[1] C. M. Urry, P. Padovani, *Unified Schemes for Radio-Loud Active Galactic Nuclei*, PASP **107** (1995) 803

[2] C. Tadhunter, *An introduction to active galactic nuclei: classification and unification*. New Astronomy Reviews **52** (2008) 227

[3] M. P. Hobson, G. P. Efstathiou, A. N. Lasenby, *General Relativity: An Introduction for Physicists*. Cambridge University Press (2006).

[4] R. D. Baldi, *The Birth, Life and Death of Active Galactic Nuclei in radio galaxies*. PhD Thesis, Università degli Studi di Torino (2009).

[5] P. Padovani, *High Energy Emission from AGN and Unified Schemes*. Talk at the Vulcano Workshop "Frontier Objects in Astrophysics and Particle Physics", Invited Review at the Vulcano Workshop 1998 'Frontier Objects in Astrophysics and Particle Physics', F. Giovannelli and G. Mannocchi eds., SIF, Volume 65, p. 159

[6] J. H. Fan, *Relation between BL Lacertae Objects and Flat-Spectrum Radio Quasars*. ApJ **585** (2003) L23

[7] A. Loeb, E. Waxman, *Cosmic gamma-ray background from structure formation in the intergalactic medium*. Nature **405** (2000) 156

[8] P.F. Michelson, W. B. Atwood, S. Ritz, *Fermi Gamma-Ray Space Telescope: High-Energy Results from the First Year*. Rep. Prog. Phys. **73** (2010) 074901

[9] *The Great Observatories: Compton Gamma-Ray Observatory*. Scientific American (1999), `http://www.scientificamerican.com/article/the-great-observatories-c/`

[10] G. J. Fishman, D. H. Hartmann, *Gamma-ray Bursts: New observations illuminate the most powerful explosions in the universe*. Scientific American **34** (1997, July issue) 68

[11] N. Gehrels, J. Paul, *The New Gamma-Ray Astronomy*. Physics Today (1998, February issue) 26

[12] *NASA's Great Observatories*. (2004) `http://science.nasa.gov/missions/cgro/`

[13] W. B. Atwood et al., *The Large Area Telescope on the* Fermi Gamma-Ray Space Telescope *Mission*. ApJ **697** (2009) 1071

[14] C. Meegan, MSFC, *Gamma-ray Burst Monitor (GBM)* (2011) `http://fermi.gsfc.nasa.gov`

[15] A. Tramacere, C. Vecchio, *γ-ray DBSCAN: a clustering algorithm applied to* Fermi-*LAT γ-ray data. - Detection performances with real and simulated data*, in HIGH ENERGY GAMMA-RAY ASTRONOMY: 5th International Meeting on High Energy Gamma-Ray Astronomy. AIP Conference Proceedings, Volume 1505, pp. 705-708 (2012)